Supplementary Information for:

Title: Structure and dynamics of the essential endogenous mycobacterial polyketide synthase Pks13.

Authors: Sun Kyung Kim[1,9], Miles Sasha Dickinson[1,2,9], Janet Finer-Moore[1], Ziqiang Guan[3], Robyn M. Kaake[4,7,8], Ignacia Echeverria[7,8], Jen Chen[1], Ernst H. Pulido[4], Andrej Sali[5], Nevan J. Krogan[4,7,8], Oren S. Rosenberg[1,6*], Robert M. Stroud[1,2*]

Affiliations:

[1]Department of Biochemistry and Biophysics, University of California San Francisco, San Francisco, CA 94143, U.S.A.

[2]Chemistry and Chemical Biology Graduate Program, University of California San Francisco, San Francisco, CA 94143, U.S.A.

[3] Department of Biochemistry, Duke University Medical Center, Durham, NC 27710

[4] Gladstone Institute of Data Science and Biotechnology, J. David Gladstone Institutes, San Francisco, California, U.S.A.

[5] Department of Bioengineering and Therapeutic sciences

[6] Department of Medicine, Division of Infectious Diseases, University of California, San Francisco, San Francisco, U.S.A.

[7]Department of Cellular and Molecular Pharmacology, University of California, San Francisco, San Francisco, California, U.S.A.

[8]Quantitative Biosciences Institute, University of California, San Francisco, San Francisco, California, U.S.A.

[9]These authors contributed equally

This PDF file includes:

Supplementary Text

Comparison of the KS-AT arrangement with other structures of isolated KS-AT.

There are other structures of KS-AT paired domains from type I PKSs and FASs. Pks13 AT domains are arched 'downward' from the KS dimer by some 15° relative to the arrangement seen in type I PKS 6-deoxyerythronolide B synthase (DEBS) 2 module 3[1], DEBS 3 module 5[1–5], or porcine and human FASs[6–8] (Fig S12A-D). When compared with the density envelope for type I pikromycin PKS module 5 (PikAIII), docking of KS and AT domains separately into their density shows that the PikAIII AT domains are rotated to arch upwards by ~120° and rotated about their longer axis[9,10] (Fig S12E). There is a unique specificity for these relative positions perhaps because of the specific differences in the downstream domains in each PKS module. Pks13 for example has a unique arrangement of domains including an ACP both before and after the KS-AT.

Comparison of ACP:KS binding modes

The KS delivery conduit observed in the Pks13 structure near the ACP1b position is the same tunnel where both trans-acting and cis-acting ACPs bind to their cognate KSs. Trans-acting ACPs from type II PKSs, AntF[11] and Iga10[12], and from *E. coli* fatty acid synthase, AcpP[13,14], have been shown to interact similarly with their cognate KS domains via helix II, with the Ppant-binding serine residue at the N-terminus of helix II pointing towards the substrate delivery conduit (Fig S13A-D). The Pks13 ACP1b is unlikely to adopt this pose to deliver substrate to the KS considering the length constraints of the ACP-KS linking DE-rich linker, since it would entail an approximate 180° rotation about an axis connecting the ACP1b and KS active sites (Fig S13A-D).

Structures indicate that during substrate elongation in type I modular PKSs DEBS module 1[15] and Lsd14[16], cis-acting ACPs bind near the delivery conduit at the KS dimer interface in a cleft between KS dimer, and KS-AT linker and AT domains of the same protomer (Fig S13E,F). In this position, loop 1 and helix II of ACP interact with the KS dimer, with loop 1 mediating most of the interaction. In both structures, the Ppant arm attached to the ACP stretches into the conduit next to the catalytic C267 of the opposite KS protomer. In Pks13, ACP1b, which resides at the N-terminus

of the same polypeptide chain as the KS and delivers the meromycolate chain onto the KS of the same protomer, similarly binds near the cleft between the KS-KS' dimer, the KS-AT linker' and AT' domains (Extended Fig 7, Fig S13E,F).

In the cryoEM structure of pikromycin PKS module 5 (PikAIII)[9,10], ACP4 from the previous module 4, fused with a flexible linker to the docking domain of module 5, binds on the 'bottom' of the KS domain (as viewed in Fig 1C left). ACP4 would deliver the growing polyketide from the previous module to the KS active site, hence it is functionally analogous to ACP1 in Pks13, but whereas PikAIII ACP4 operates in *trans*, ACP1 operates in *cis* and its position is constrained by the ACP1-KS linker. It was proposed[9] that the ACP4 serine is next to a side active-site entrance analogous to the lipid delivery conduit in Pks13, but in Pks13 this ACP position is sterically occluded by AT. Furthermore, the electrostatic interactions between KS and the DE-rich linker guide ACP1 to the two different sites (i.e. ACP1a and ACP1b) seen in the Pks13 structure and to the docked position of ACP1b at the delivery conduit in KS (Fig 1D, S11A).

ACP5 of PikAIII, which brings the extender unit from the AT active site to the KS active site, binds at the 'top' of the KS viewed from the Fig 1C orientation, near the KS lipid conduit[10] when loaded with methylmalonyl. ACP5 has a function analogous to the ACP2 in Pks13. Density for ACP2 is not defined as such in our EM map, but the KS lipid conduit is accessible to the low-resolution lenticular shaped densities we ascribe to the ACP2 and domains C-terminal to it. Thus, ACP2 could deliver the second R2 substrate (C24-C26) through this tunnel. In the Pks13 structure, this KS lipid conduit tunnel is occupied by the meromycolyl acyl chain, therefore it would need to widen to accept the incoming R2 to undergo the condensation with R1 in the KS domain. This mechanism is eminently reasonable, as the product of the condensation must be taken out of the site on ACP2 through a topologically accessible pathway, without restriction. Low-resolution solution structures of Pks13 without bound substrates are similar to our cryoEM structure, except that the Pks13 is primarily monomeric, suggesting that the dimer interface may be flexible enough to dissociate at the lipid conduit to widen the conduit for R2 access[17].

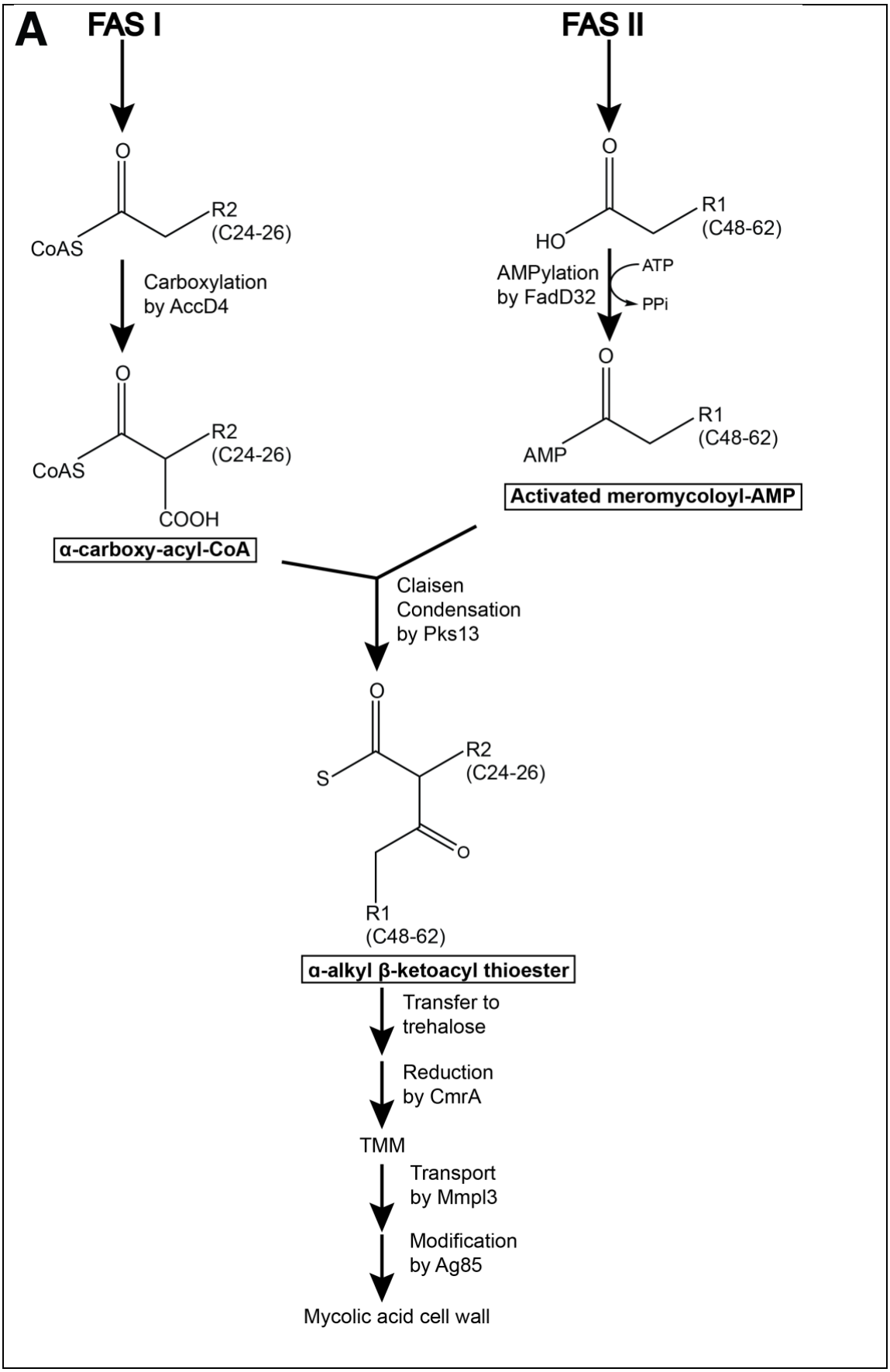
A
FAS I
FAS II
O
R2
(C24-26)
CoAS
Carboxylation
by AccD4
COOH
α-carboxy-acyl-CoA
HO
R1
(C48-62)
AMPylation
by FadD32
ATP
PPi
AMP
Activated meromycoloyl-AMP
Claisen
Condensation
by Pks13
S
α-alkyl β-ketoacyl thioester
Transfer to
trehalose
Reduction
by CmrA
TMM
Transport
by Mmpl3
Modification
by Ag85
Mycolic acid cell wall

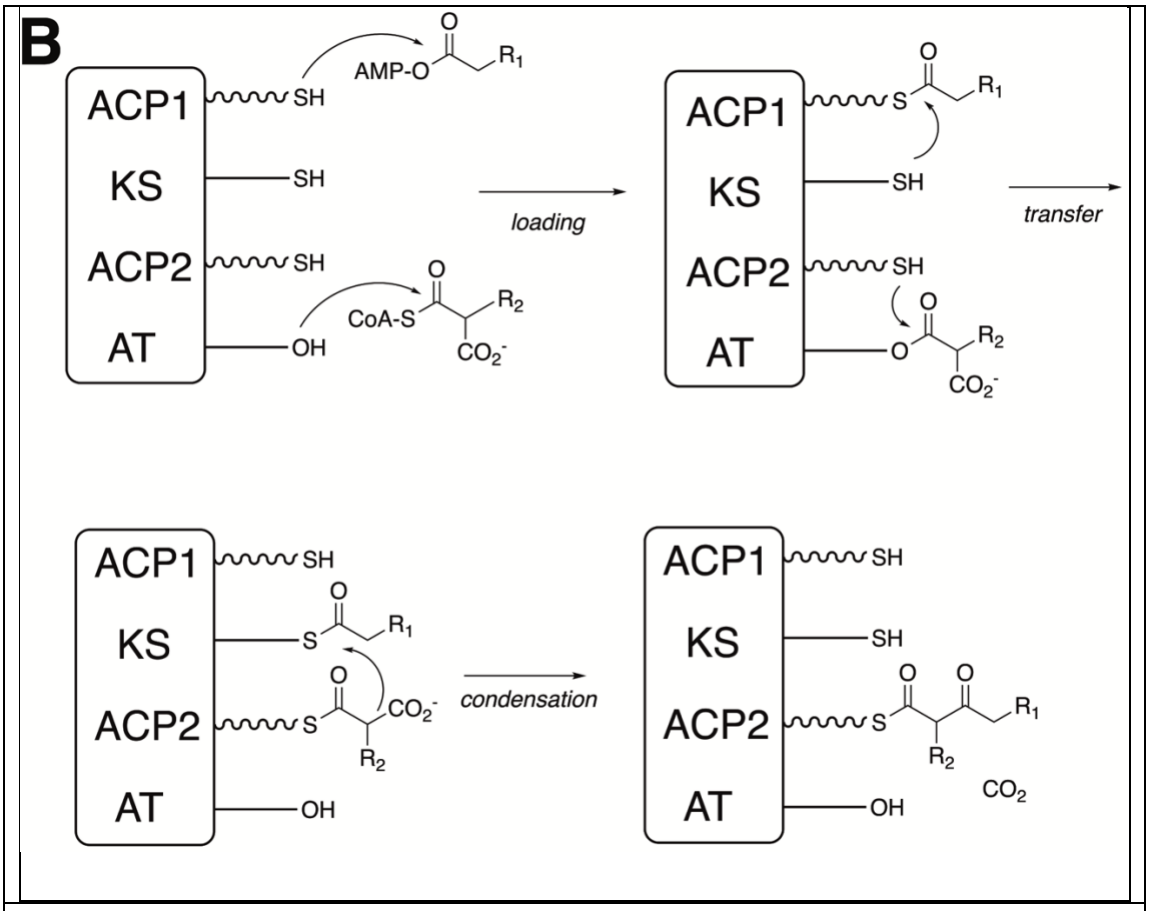

Fig S1. An Overview of mycolic acid synthesis pathway in mycobacteria.

(A) FAS I and FAS II synthesize the precursor fatty acids that are condensed by Pks13 to produce α-alkyl β-ketoacyl thioester, a direct precursor of mycolic acids. Long-chain acyl-CoA (C24-C26) is produced by FAS I and carboxylated by AccD4 to produce α-carboxyacyl-CoA. FAS II, composed of multiple enzymes, produces the acyl backbone for the meromycolyl chain. The mature C48-C62 meromycolyl chain is activated by FadD32 to produce meromycolyl-AMP. Pks13 carries out decarboxylative Claisen condensation of the two fatty acids to produce α-alkyl β-ketoacyl thioester. α-alkyl β-ketoacyl thioester is transferred to trehalose and reduced by CmrA to produce trehalose monomycolate (TMM). The product is transported across the plasma membrane by Mmpl3 and is further modified by the Ag85 complex

to form the final building blocks of mycolic acid cell wall. (B) The chemical reactions carried out by the Pks13 domains are indicated. The reactions can occur in *trans* between domains of alternate polypeptide chains.

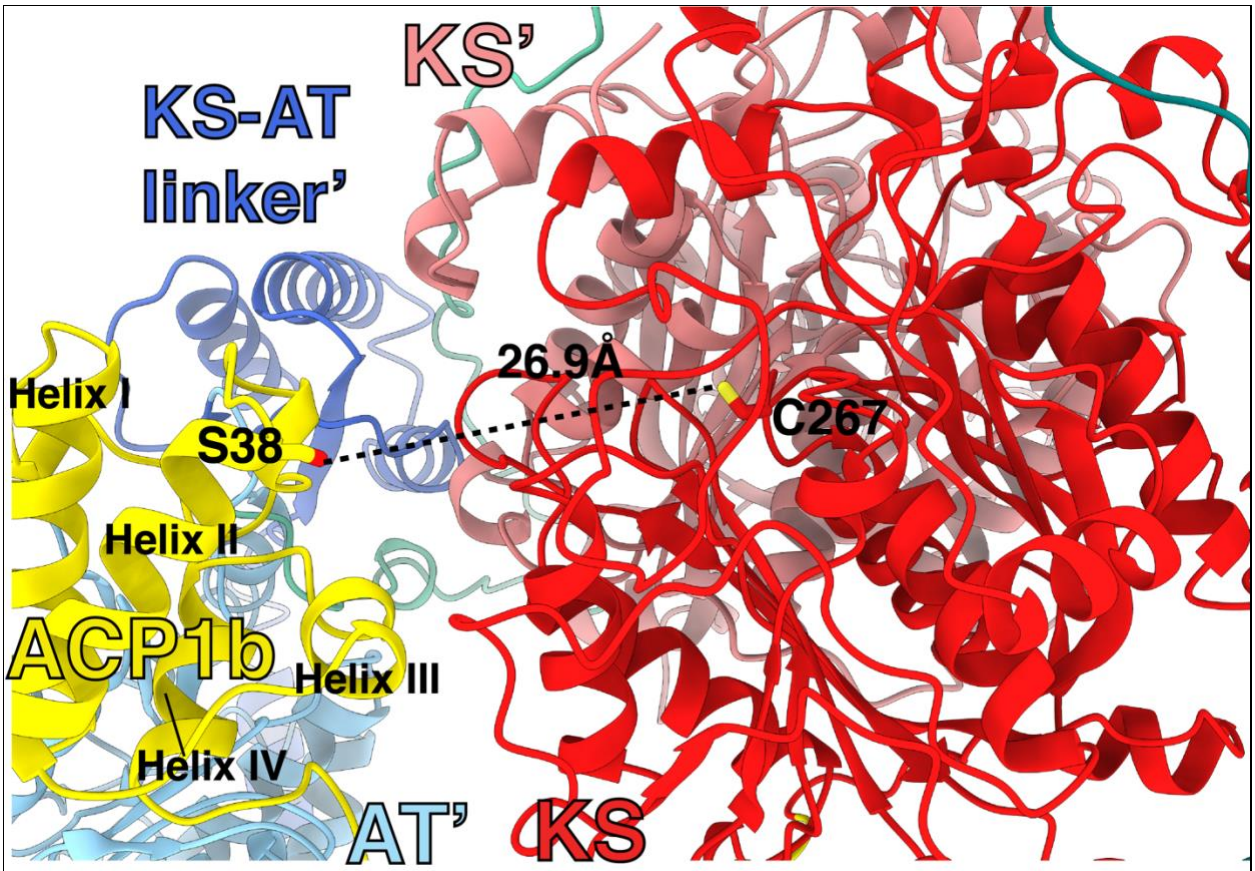

Supplementary Fig 2. Distance between ACP1b S38 and KS C267. ACP1b S38, which receives the Ppant arm, is 27 Å away from the KS active site C267 of the same protomer.

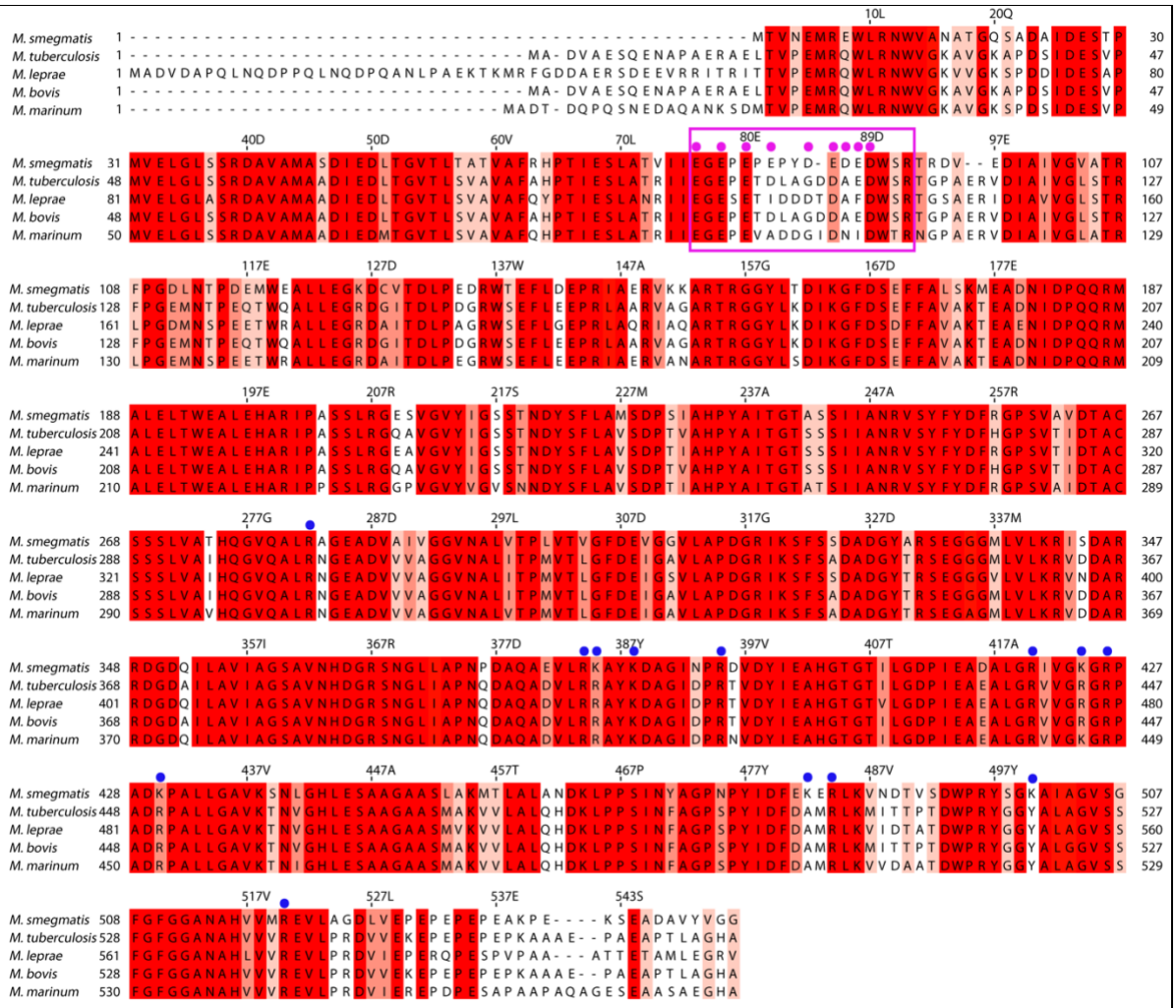

Supplementary Fig 3. Sequence alignment of Pks13 ACP1 to KS region across mycobacterial species. The DE-rich linker region is boxed in magenta with aspartic acid and glutamic acid residues labeled with magenta dots. Lysine and arginine residues making up the positively charged surfaces in the KS domain are labeled with blue dots (shown in Fig 1D, ~~S6-8~~/Extended Fig 3-5). Pks13 protein sequences from five different mycobacterial species are aligned from N-terminus to the end of the KS domain. Sequence numbering above the sequences is for *Ms.* Residues were colored by conservation with highly conserved residues in dark red and less conserved residues in lighter colors. Alignment was carried out using Clustal Omega[18] and annotations were made in Jalview[19] .

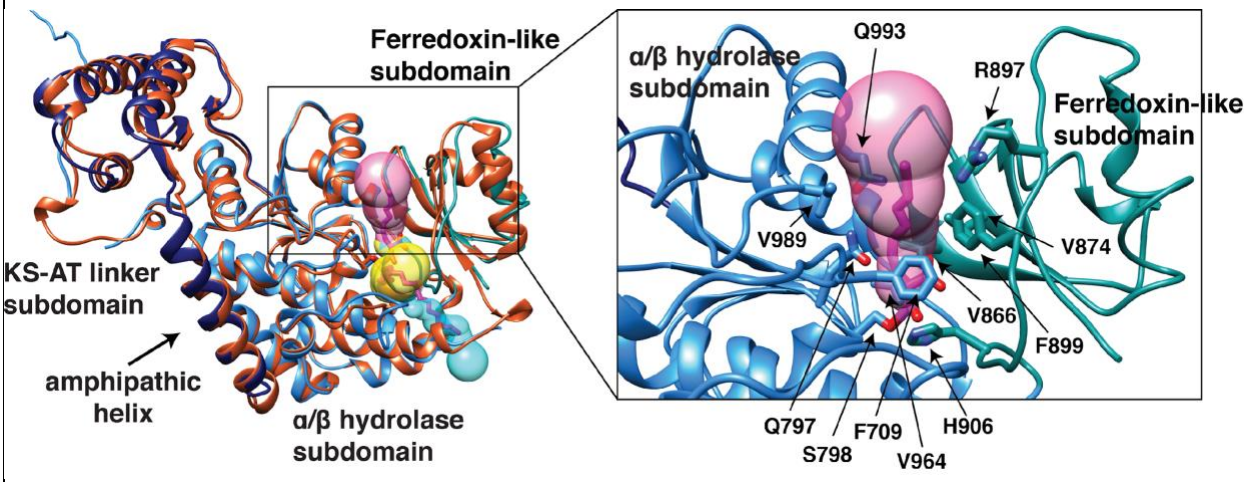

Supplementary Fig 4. Comparison of carboxyacyl substrate positions between *Mtb* and *Ms* Pks13 AT domains. Left: *Ms* Pks13 AT structure (KS-AT linker subdomain; navy blue, αβ-hydrolase subdomain; blue, and ferredoxin-like subdomain; cyan) is overlaid with *Mtb* Pks13 AT fragment structure (PDB:3TZZ[20], orange all throughout), resulting in 1.00 Å RMSD over 449 Cα atoms. The carboxyacyl ligand in two different positions as reported in *Mtb* Pks13 AT fragment[20] lies within the yellow and cyan hydrophobic tunnels. The native carboxyacyl substrate in our *Ms* Pks13 AT structure is seen in a different hydrophobic tunnel colored magenta. In all three cases, the serine-ester carboxyacyl substrate is colored magenta. Inset: Close-up view of the hydrophobic tunnel surrounding the native substrate in *Ms* Pks13 AT. Residues lining the tunnel are labeled. Tunnels were calculated using MOLEonline[21].

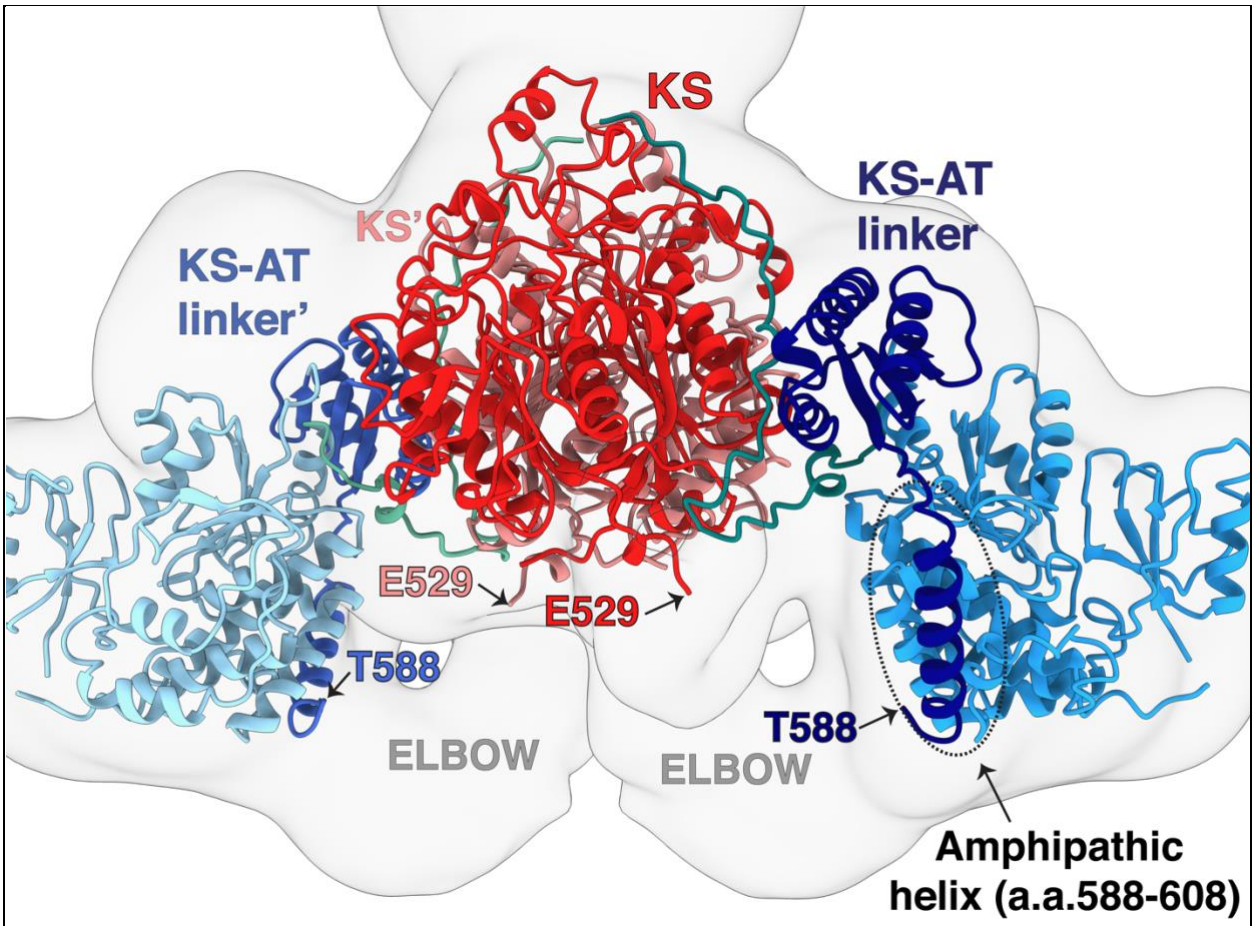

Supplementary Fig 5. View of ELBOW density, and amphipathic helix. Residues between E529 (KS) and T588 (KS-AT linker) are not modeled due to low resolution density in the region. This region is presumably connected by a flexible “ELBOW” region shown in the low-resolution density map that connects the end of E529 and beginning of T588. An amphipathic helix (588-608) found only in mycobacterial Pks13s leads into the KS-AT linker domain (circled and labeled).

Chemical Formula: $C_{55}H_{106}O_2$
Exact Mass: 798.819

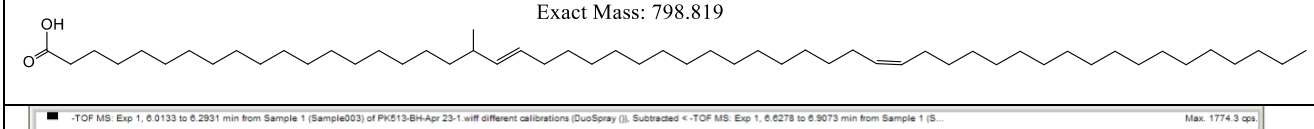

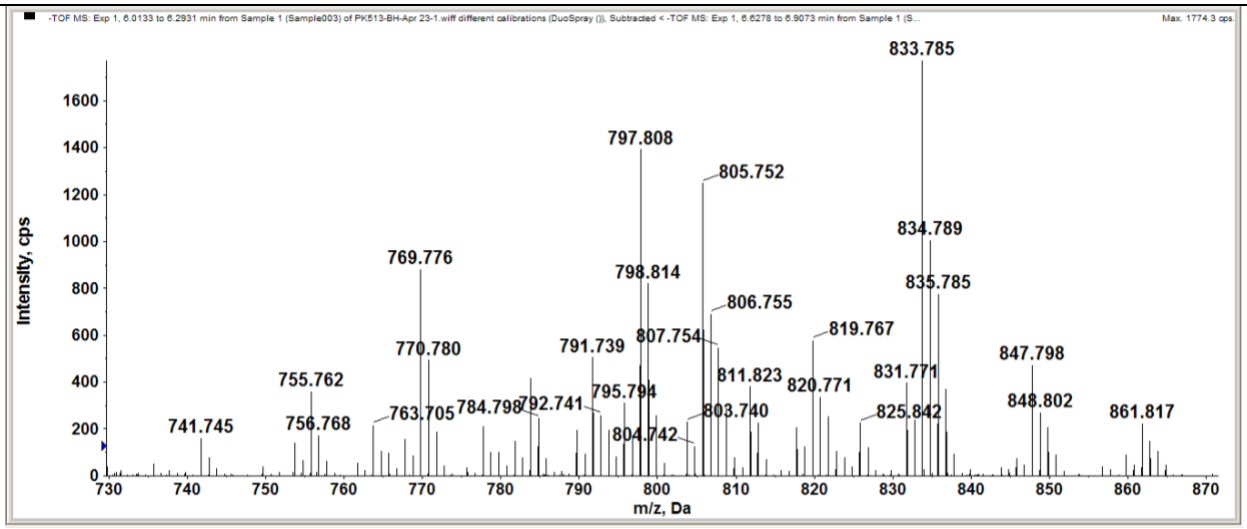

Supplementary Fig 6. The extremely long chain, C51-C57 in length, α_2-meromycolate branch has its major component with the formula $C_{55}H_{106}O_2$ with exact mass 798.819 Da. consistent with the substrate seen attached covalently to the active site of the KS domain in density. The α_2 chain contains a single methyl branch following a trans double bond, and a single cis double bond[22].

Chemical Formula: $C_{40}H_{78}O_2$
Exact Mass: 590.600

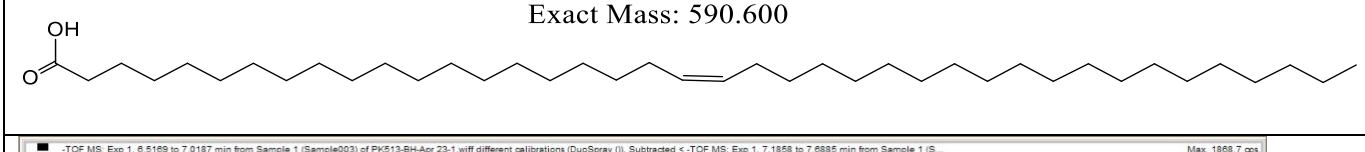

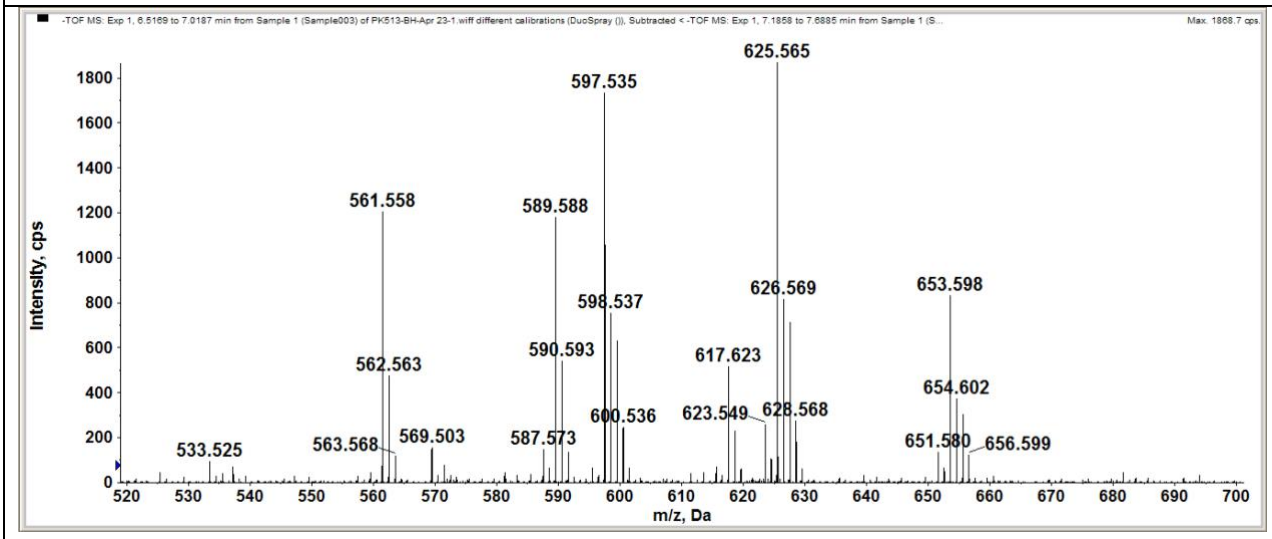

Supplementary Fig 7. The C36-C42 chain α'-meromycolate branch has its major component with the formula $C_{40}H_{78}O_2$ and exact mass 590.600, a cis-monounsaturated fatty acid similar in length to tetracontanoic acid. Mass spectra for the species are shown. This chain is consistent with the meromycolate branch of α' mycolic acid found in *M.smegmatis* but not found in *M.tuberculosis*.

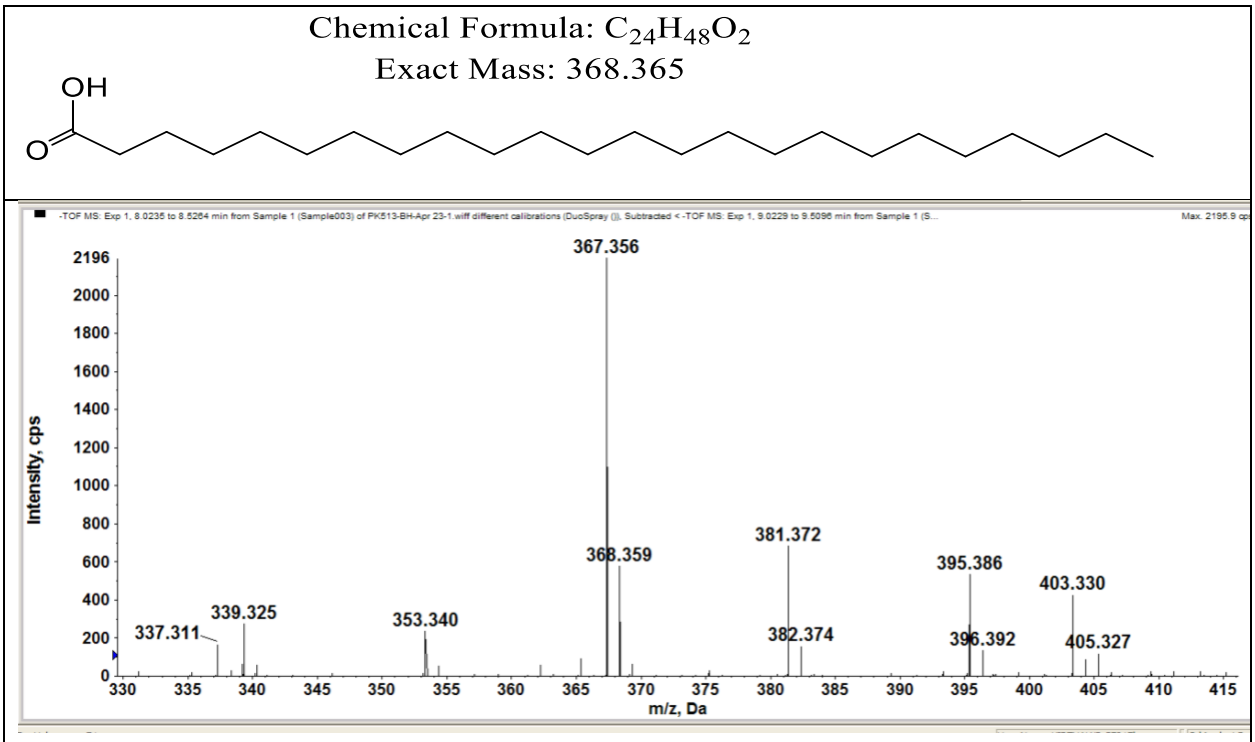

Supplementary Fig 8. The α-branch chain. Chains of the expected lengths (C22-C26) for the α-branch, the α-carboxy fatty acid, as seen attached to S798 of the AT domain. The predominant species is for C24 chain of mass 368.365 Da. The carboxyl group on the α-branch have probably been released during the hydrolysis from Pks13 or during mass spectrometry.

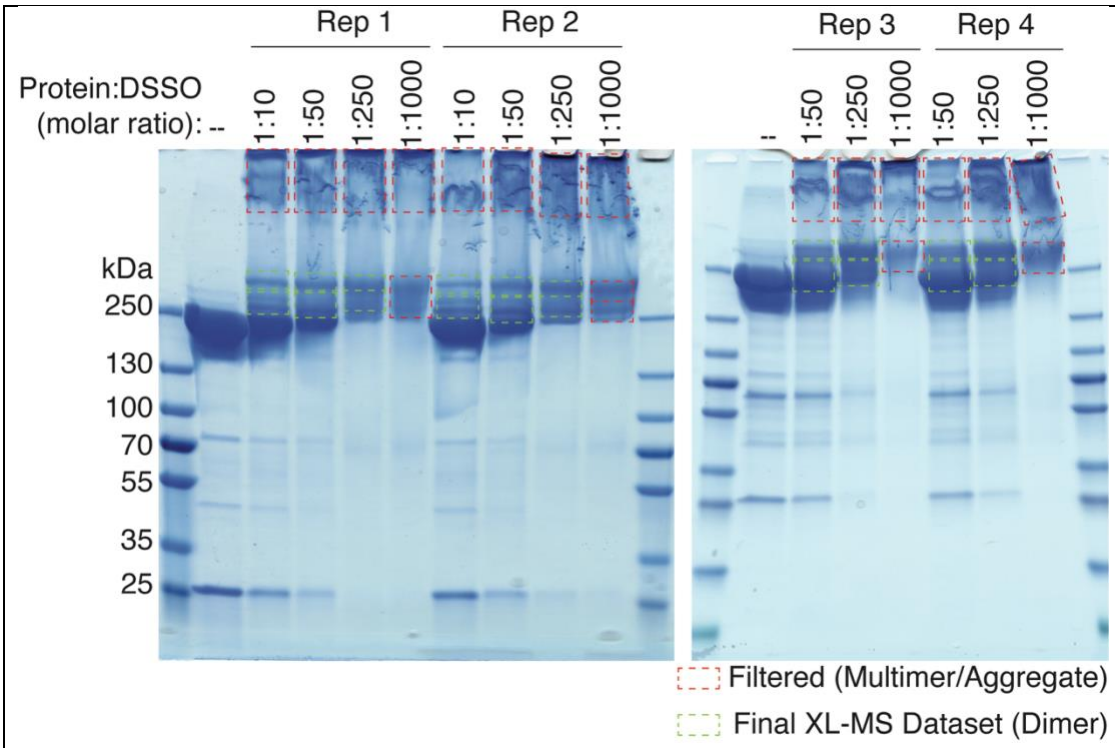

Supplementary Fig 9. SDS-PAGE separation of Pks13 cross-linked with increasing amounts of DSSO. Pks13 was cross-linked with increasing amounts of DSSO for 30min at 37°C (Rep1, 3, and 4) or 4°C (Rep2), separated on a 4-20% SDS-PAGE gel, and stained with MS safe blue stain. All non-monomeric bands were cut as indicated and analyzed by XL-MS^3 (see methods for details). Mapping linkages to the cryoEM structures (Fig S10) demonstrated high levels of distance violations for cross-links that could be mapped. Given that most of these were found in bands associated with higher amounts of cross-linking and potential aggregates, data corresponding to these bands (shown in Red) were filtered out of the Final dataset. Bands that correspond to the lower molecular weight products are shown in green.

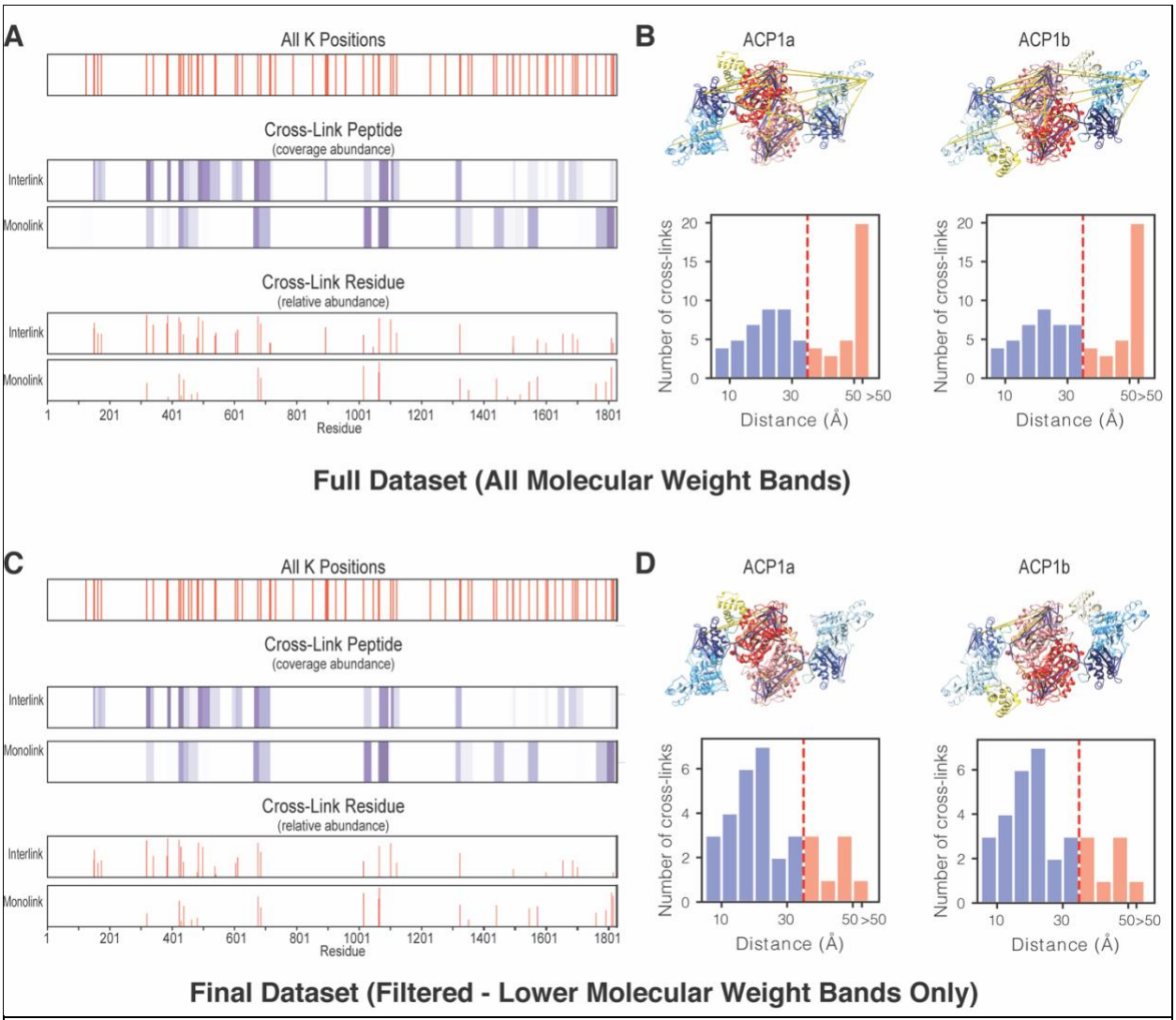

Supplementary Fig 10. Summary of Pks13 DSSO cross-links. (A, C) For the full (A) and filtered (C) data- sets all Pks13 lysine positions (K positions) are plotted on the top graph. The cross-linked peptide coverage is shown for interlinks and monolinks as an intensity plot with darker purple indicating higher spectral count. The corresponding relative abundance for each cross-link by residue is shown as a line graph in the two plots below. (B, D) DSSO interlinked residues are mapped to the two cryo-EM structures (shown on the top) for the full (**B**) and filtered (**D**) data- sets. Linkages that satisfy the expected distance (<35Å) are shown in blue, and linkages that violate this distance are shown in yellow. Histograms that plot the distances for each of the unique linkages are shown for each structure (shown on the bottom).

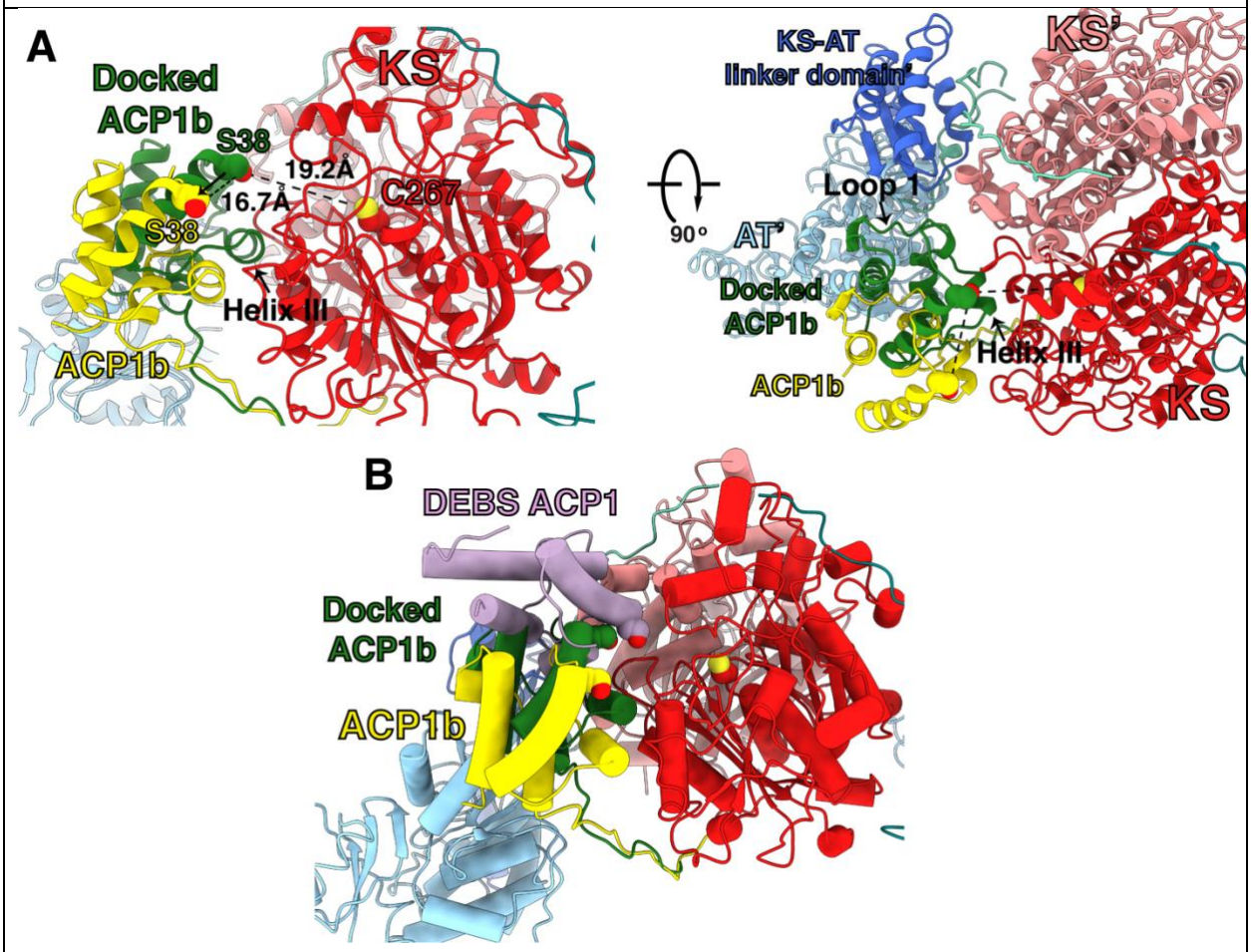

Supplementary Fig 11. ACP1b substrate delivery docked position. (A) S38 of docked ACP1b (green), which is required to deliver the meromycolate to the KS, is removed ~17 Å from the S38 of our ACP1b structure (yellow). From the docked ACP1b position (green), S38 is ~19 Å from the catalytic C267 of KS. In this docked position, helix III and loop 1 make contacts with the KS-KS' dimer and KS-AT linker' and AT' domains. (B) Superposition of ACP1b, ACP1b docked position, and DEBS ACP1. Docked ACP1b orientation is ~90° rotated from the DEBS module 1 ACP binding mode.

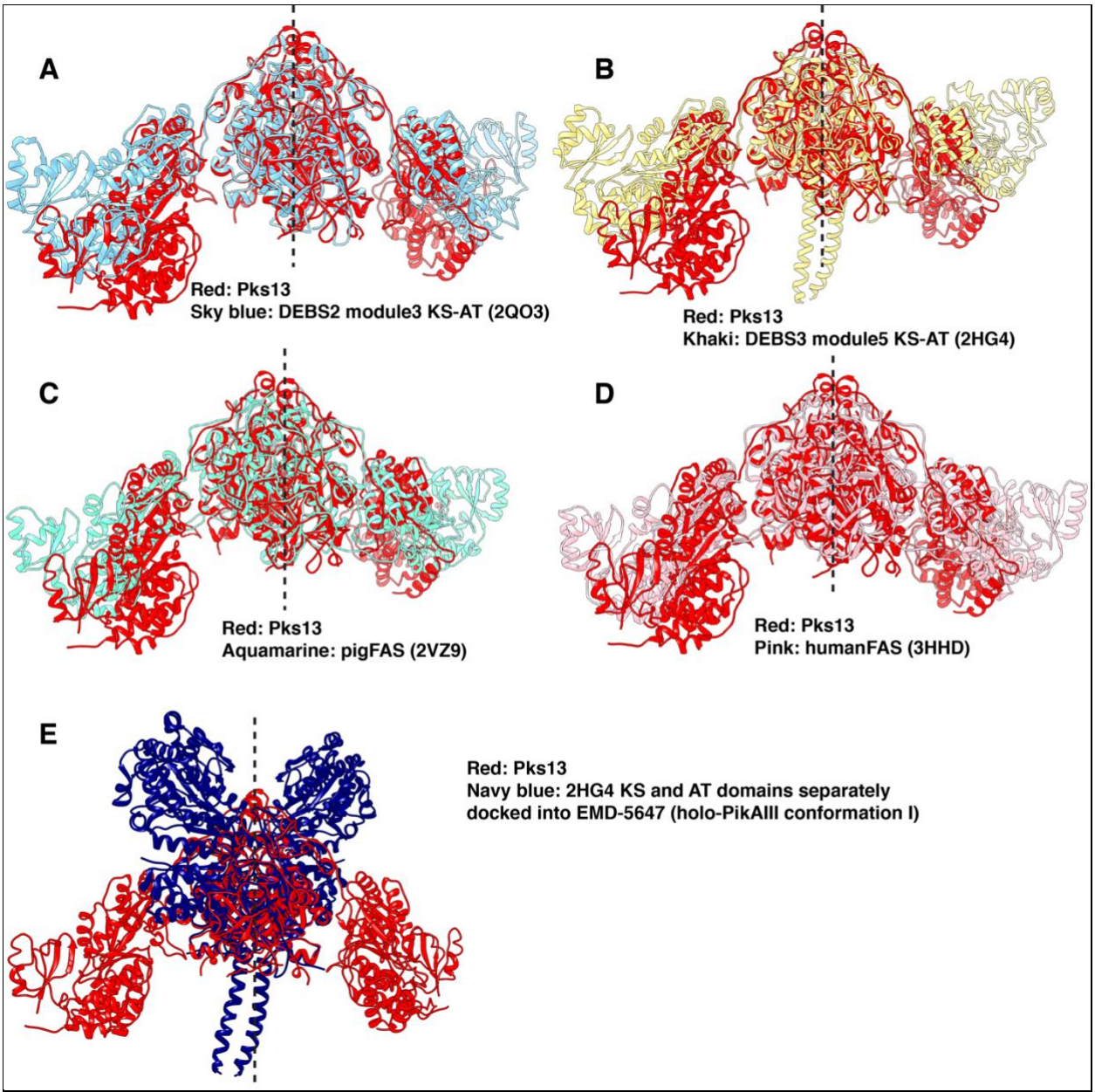

Supplementary Fig 12. Pks13 KS-AT comparisons to other structures that include the di-domain KS-AT. (A) Comparison of Pks13 KS-AT (red) to that in module 3 of DEBS 2 (blue) (PDB: 2QO3). (B) Comparison of KS-AT in Pks13 (red) to that in module 5 of DEBS 3 (khaki) (2HG4). (C) Comparison of KS-AT in Pks13 to that in porcine FAS (Aquamarine) (2VZ9). (D) Comparison of KS-AT in Pks13 (red) to that of human FAS (pink) (3HHD). (E)

Comparison of KS-AT in Pks13 (red) to a structure of PikAIII (blue) obtained by fitting domain homology models into cryo-EM density.

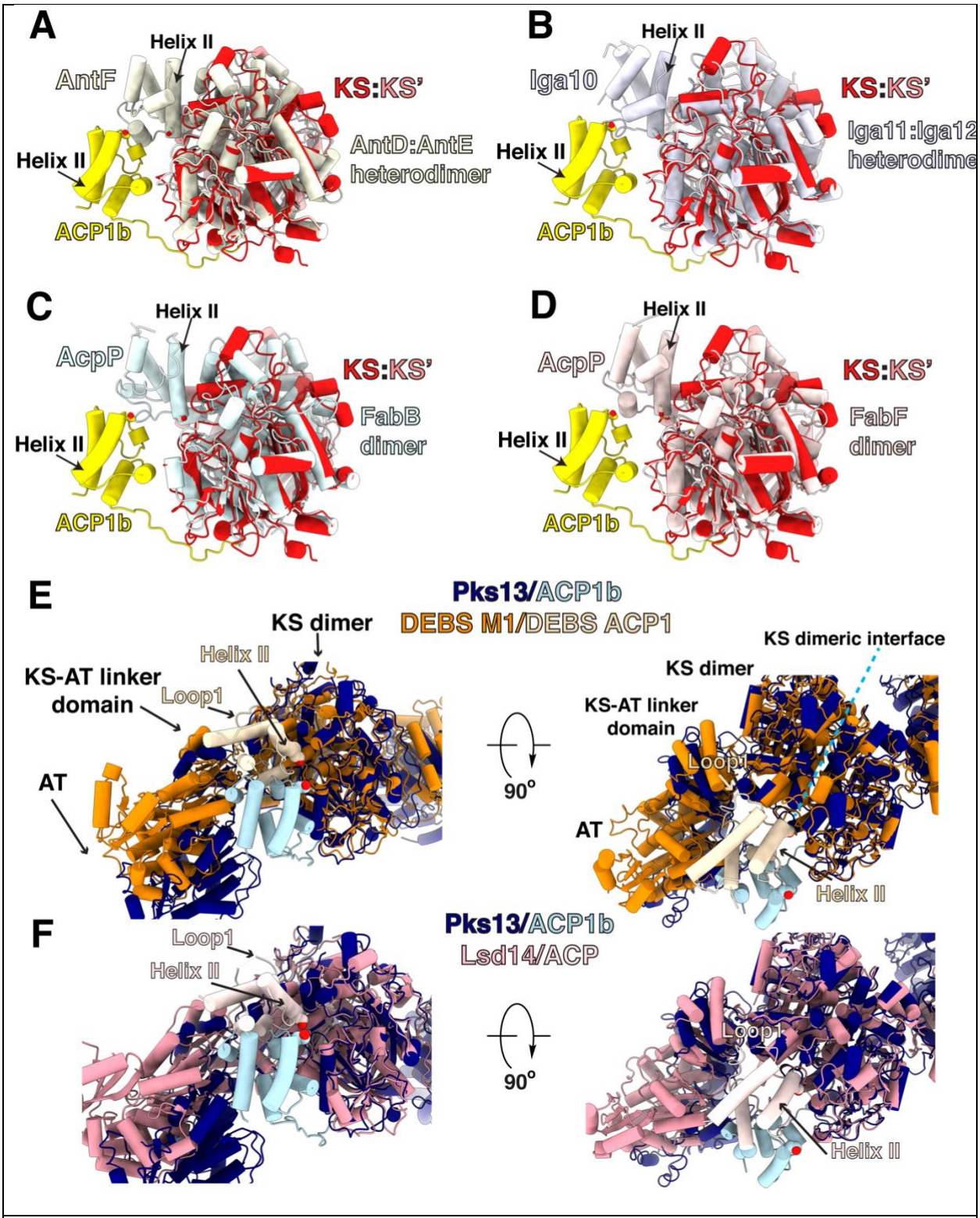

Supplementary Fig 13. Comparison of ACP:KS binding modes. Superposition of Pks13 ACP1b:KS structure with trans-acting ACPs (A) AntF, (B) Iga10, and (C, D) AcpP and their cognate KSs (same

color as cognate ACPs). These trans-acting ACPs interact with their KSs similarly via their helix II, with their Ppant-binding serine at the N-terminus of helix II shown in stick representation. Superposition of ACP1b: Pks13 structure with cis-acting ACPs from (E) DEBS module 1and (F) Lsd14 PKSs interacting with their cognate PKS module. KS interacting epitopes loop1 and helix II on the DEBS and Lsd14 ACP are labeled, and Ppant-binding serine is shown as sphere at the N-terminus of helix II of ACPs.

Table S1 Exact mass measurement of fatty acids bound to Pks13					
Fatty acids are detected as deprotonated $[M-H]^-$ or chloride adduct $[M+Cl]^-$ ions					
		$[M-H]^-$		$[M+Cl]^-$	
		Expected *m/z*	Observed *m/z*	Expected *m/z*	Observed *m/z*
C22-C26	C22	339.327	339.325		
	C23	363.343	363.341		
	C24	367.358	367.356	403.334	403.330
	C25	381.374	381.372		
	C26	395.389	395.385		
C36-C42	C36	533.530	533.525	569.506	569.503
	C38	561.562	561.558	597.538	597.535
	C40	589.593	589.588	625.569	625.565
	C42	617.624	617.623	653.600	653.598
C51-C57	C51	741.747	741.745	777.726	777.724
	C52	755.765	755.762	791.741	791.739
	C53	769.781	769.776	805.757	805.752
	C54	783.796	783.793	819.772	819.767
	C55	797.812	797.808	833.788	833.785
	C56	811.828	811.823	847.804	847.798
	C57	825.843	825.842	861.819	861.817

Table S2. Summary of unique Pks13 inter-linked residues excluding files from highly cross-linked samples. Submitted digitally as a separate excel spreadsheet.

Table S3. Metadata all DSSO cross-linked Pks13 XL-MS files. Submitted digitally as a separate excel spreadsheet.

Table S4. Summary of the Pks13 dimer integrative structure modeling. To assess the convergence of model scores and determine the sampling precision we used a Kolmogorov-Smirnov two-sample test statistic to compare the distribution of scores and a χ2-test (one-sided) for homogeneity of proportions between two independent sets of samples.

1) Gathering information	
Prior models	2-fold symmetry derived from cryo-EM structure
Physical principles and statistical preferences	Excluded volume Sequence connectivity
Experimental data	57 DSS0 Atomic structure from cryo-EM map; PDB TBD
2) Representing the system	
Atomic (structured) components	Pks13: 1-76, 89-228, 229-232, 233-529, 588-835, 836-838, 839-1074, 1078-1173, 1238-1356, 1461-1535, 1539-1816, 1-76, 89-228, 229-232, 233-529, 588-835, 836-838, 839-1074, 1078-1173, 1238-1356, 1461-1535, 1539-1816
Unstructured components	Pks13: 77-88, 530-587, 1075-1077, 1174-1237, 1357-1460, 1536-1538, 77-88, 530-587, 1075-1077, 1174-1237, 1357-1460, 1536-1538
Resolution of structured components	1 [R1] residue per bead
Resolution of unstructured components	10 [R10] residues per bead
Structural coverage	86.77 %
Rigid body (RB) definitions	RB1: $Pks13_{1-76}$ RB2: $Pks13_{89-228}$,$Pks13_{229-232}$,$Pks13_{233-529}$,$Pks13_{588-835}$,$Pks13_{8}$ RB3: $Pks13_{1078-1173}$ RB4: $Pks13_{1238-1356}$ RB5: $Pks13_{1461-1535}$ RB6: $Pks13_{1539-1816}$ RB7: $Pks13_{1-76}$ RB8: $Pks13_{89-228}$,$Pks13_{229-232}$,$Pks13_{233-529}$,$Pks13_{588-835}$,$Pks13_{8}$ RB9: $Pks13_{1078-1173}$ RB10: $Pks13_{1238-1356}$ RB11: $Pks13_{1461-1535}$ RB12: $Pks13_{1539-1816}$
Resolution of disordered regions	10 [R10] residues per bead
Composition (number of copies of Pks13)	2
Spatial restraints encoded into scoring function	Excluded volume; applied to the R1 representation Sequence connectivity; applied to the R1 representation Cross-link restraints; applied to the R1 representation
3.1) Enumeration of threading of degrees of freedom	
3.2) Structural Sampling	
Sampling method	Replica Exchange Gibbs sampling, based on Metropolis Monte Carlo
Replica exchange temperature range	1.0 - 2.5
Number of replicas	8
Number of runs	100
Number of structures generated	2500000
Movers for flexible string of bead	Random translation up to 4.0 Å
CPU time	22 hours on 80 processors
4.1) Validating the threading models	
4.2) Validating the Pom152 ring models	
Models selected for validation	
Number of models after equilibration	2500000
Number of models that satisfy the input information	229554
Number of structures in samples A/B	112886/116668
p-value of non-parametric Kolmogorov-Smirnov two-sample test	0.02 (threshold p-value > 0.05)
Kolmogorov-Smirnov two-sample test statistic, D	1.0
Thoroughness of the structural sampling	
Sampling precision	61.37 Å
Homogeneity of proportions χ^2 test (p-value)/Cramers V value	0.000/0.067 (thresholds: p-value>0.05 OR Cramer's V<0.1)
Number of clusters	3
Cluster precisions	cluster 1 : 55.0 % cluster 2 : 21.7 %

Table S5. Table with description and scores for overall DSSO cross-linked peptides for all processed files including inter-linked, mono-linked, and single peptides. Submitted digitally as a separate excel spreadsheet.

Table S6. Summary of all unique Pks13 inter-linked residues from the full dataset. Submitted digitally as a separate excel spreadsheet.

Movie S1 caption: Relative positions of the ACP1, KS, AT domains, and substrates determined by cryoEM. Scene 1. KS-AT didomain: The high-resolution density map is superposed onto the KS-AT dimer. The 2-fold axis is vertical. The density for the HINGE domain on top of the KS dimer is not interpretable at atomic resolution. Scene 2. ACP1a and ACP1b structures overlaid: Low-resolution envelope is around the 'cartoon' representation of the overlaid ACP1a-KS-AT and ACP1b-KS-AT structures. The two-fold axis is vertical. The envelope for the DE-rich linker sequence that connects the ACP1 and the KS is clearly delineated. Scene 3. View of ACP1a, ACP1b, KS lipid delivery conduit, and AT lipid conduit: The molecular surface is shown on the KS and AT domains. The view starts from the ACP1a showing the attachment point of the Ppant arm at S38, then moves to the ACP1b location where S38 is highlighted. Next, the view peers into the KS lipid delivery conduit which leads into the KS active site where the covalently bound mycolic acid substrate rises vertically from the sulfur of C267. Active site residues are shown as sticks. The view pulls back to give the relative context of the AT active site serine S798 bound to its α-carboxy-fatty acid substrate. Active site residues are shown as sticks. Scene 4. AT morphing between AT_{in} and AT_{out} structures: A cartoon showing the 'liquorice' style rendering of the motion of one AT domain relative to the KS dimer from focused alignments, viewed from the side nearest the AT domain with the KS dimer kept constant in position to emphasize the domain shift. This is followed by the same events

viewed down the 2-fold axis between the KS domains that illustrates the ~7° rotation and twist associated with this motion.

Supplementary material references

1. Tang, Y., Chen, A. Y., Kim, C.-Y., Cane, D. E. & Khosla, C. Structural and mechanistic analysis of protein interactions in module 3 of the 6-deoxyerythronolide B synthase. *Chem. Biol.* **14,** 931–943 (2007).
2. Tang, Y., Kim, C.-Y., Mathews, I. I., Cane, D. E. & Khosla, C. The 2.7-Angstrom crystal structure of a 194-kDa homodimeric fragment of the 6-deoxyerythronolide B synthase. *Proc. Natl. Acad. Sci. USA* **103,** 11124–11129 (2006).
3. Edwards, A. L., Matsui, T., Weiss, T. M. & Khosla, C. Architectures of whole-module and bimodular proteins from the 6-deoxyerythronolide B synthase. *J. Mol. Biol.* **426,** 2229–2245 (2014).
4. Khosla, C., Tang, Y., Chen, A. Y., Schnarr, N. A. & Cane, D. E. Structure and mechanism of the 6-deoxyerythronolide B synthase. *Annu. Rev. Biochem.* **76,** 195–221 (2007).
5. Khosla, C. Structures and mechanisms of polyketide synthases. *J. Org. Chem.* **74,** 6416–6420 (2009).
6. Maier, T., Leibundgut, M. & Ban, N. The crystal structure of a mammalian fatty acid synthase. *Science* **321,** 1315–1322 (2008).
7. Pappenberger, G. *et al.* Structure of the human fatty acid synthase KS-MAT didomain as a framework for inhibitor design. *J. Mol. Biol.* **397,** 508–519 (2010).
8. Leibundgut, M., Jenni, S., Frick, C. & Ban, N. Structural basis for substrate delivery by acyl carrier protein in the yeast fatty acid synthase. *Science* **316,** 288–290 (2007).
9. Whicher, J. R. *et al.* Structural rearrangements of a polyketide synthase module during its catalytic cycle. *Nature* **510,** 560–564 (2014).
10. Dutta, S. *et al.* Structure of a modular polyketide synthase. *Nature* **510,** 512–517 (2014).
11. Bräuer, A. *et al.* Structural snapshots of the minimal PKS system responsible for octaketide biosynthesis. *Nat. Chem.* **12,** 755–763 (2020).
12. Du, D. *et al.* Structural basis for selectivity in a highly reducing type II polyketide synthase. *Nat. Chem. Biol.* **16,** 776–782 (2020).
13. Milligan, J. C. *et al.* Molecular basis for interactions between an acyl carrier protein and a ketosynthase. *Nat. Chem. Biol.* **15,** 669–671 (2019).
14. Mindrebo, J. T. *et al.* Gating mechanism of elongating β-ketoacyl-ACP synthases. *Nat. Commun.* **11,** 1727 (2020).
15. Cogan, D. P. *et al.* Mapping the catalytic conformations of an assembly-line polyketide synthase module. *Science* **374,** 729–734 (2021).
16. Bagde, S. R., Mathews, I. I., Fromme, J. C. & Kim, C.-Y. Modular polyketide synthase contains two reaction chambers that operate asynchronously. *Science* **374,** 723–729 (2021).
17. Bon, C. *et al.* Solution structure of the type I polyketide synthase Pks13 from Mycobacterium tuberculosis. *BMC Biol.* **20,** 147 (2022).
18. Madeira, F. *et al.* The EMBL-EBI search and sequence analysis tools APIs in 2019. *Nucleic Acids Res.* **47,** W636–W641 (2019).
19. Waterhouse, A. M., Procter, J. B., Martin, D. M. A., Clamp, M. & Barton, G. J. Jalview Version 2--a multiple sequence alignment editor and analysis workbench. *Bioinformatics* **25,** 1189–1191 (2009).
20. Bergeret, F. *et al.* Biochemical and structural study of the atypical acyltransferase domain from the mycobacterial polyketide synthase Pks13. *J. Biol. Chem.* **287,** 33675–33690 (2012).

21. Pravda, L. *et al.* MOLEonline: a web-based tool for analyzing channels, tunnels and pores (2018 update). *Nucleic Acids Res.* **46,** W368–W373 (2018).
22. Barry, C. E. *et al.* Mycolic acids: structure, biosynthesis and physiological functions. *Prog. Lipid Res.* **37,** 143–179 (1998).